ACS Catalysis

Research Article

Cite This: ACS Catal. 2019, 9, 7124–7136

pubs.acs.org/acscatalysis

Dynamics of Reactive Species and Reactant-Induced Reconstruction of Pt Clusters in Pt/Al_2O_3 Catalysts

Michele Carosso,[†] Eleonora Vottero,[†,‡] Andrea Lazzarini,[†,§] Sara Morandi,[†] Maela Manzoli,[∥] Kirill A. Lomachenko,[⊥] Monica Jimenez Ruiz,[‡] Riccardo Pellegrini,[#] Carlo Lamberti,[¶,▲] Andrea Piovano,[‡] and Elena Groppo*[,†]

[†]Department of Chemistry, INSTM and NIS Centre, University of Torino, via Quarello 15, I-10135 Torino, Italy

[‡]Institut Laue-Langevin (ILL), 71 avenue des Martyrs, 38000 Grenoble, France

[§]Centre for Materials Science and Nanotechnology, Department of Chemistry, University of Oslo, Sem Saelands vei 26, N-0315 Oslo, Norway

[∥]Department of Drug Science and Technology, INSTM and NIS Centre, University of Torino, Via Pietro Giuria 9, I-10125 Torino, Italy

[⊥]European Synchrotron Radiation Facility, 71 Avenue des Martyrs, CS 40220, 38043 Grenoble Cedex 9, France

[#]Chimet SpA - Catalyst Division, Via di Pescaiola 74, I-52041, Viciomaggio Arezzo, Italy

[¶]Department of Physics and CrisDi Interdepartmental Centre, University of Torino, via Pietro Giuria 1, I-10125 Torino, Italy

[▲]The Smart Materials Research Institute, Southern Federal University, Sladkova Street 178/24, Rostov-on-Don 344090, Russia

ABSTRACT: We report a complete experimental characterization of the surface Pt-hydride species on an industrial 5 wt % Pt/Al_2O_3 catalyst (average particle size of 1.4 ± 0.4 nm) under different hydrogenation/dehydrogenation conditions. By combining inelastic neutron scattering, FT-IR spectroscopy, and synchronous DRIFT/XAS/MS, we identified *n*-fold coordinated Pt-hydrides and four different types of linear Pt-hydrides characterized by different adsorption strength, whose relative proportion depends on the experimental conditions. In particular, we observed that the *n*-fold coordinated hydrides convert into linear ones upon decreasing hydrogen coverage, and vice versa, and we traced this phenomenon to a morphological and electronic reconstruction of the Pt nanoparticles. Although only a fraction of the surface Pt-hydrides are directly involved in the hydrogenation of toluene, all the others play an indirect but fundamental role, maintaining the Pt nanoparticles electronically and morphologically stable during the reaction and hence avoiding the occurrence of deactivation processes. Our results, which are in good agreement with the theoretical predictions reported in the literature, offer a comprehensive picture of the dynamics of Pt nanoparticles in hydrogenation conditions. This always involves a change in the relative proportion of the Pt-hydride species, and only in some cases an electronic and morphological reconstruction of the Pt particles.

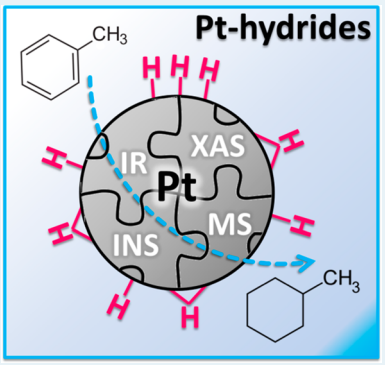

KEYWORDS: *Pt hydrides, reconstruction, DRIFT spectroscopy, XAS, INS*

1. INTRODUCTION

Pt-based heterogeneous catalysts are systems of pivotal industrial relevance, since they are employed in a wide range of industrial processes involving hydrogen, ensuring high selectivity and conversion at relatively mild operating conditions.[1−4] The key step of the process is the homolytic dissociation of molecular hydrogen at the Pt surface, with the consequent formation of different Pt-hydride species. These atomic hydrogen species are directly involved in the hydrogenation (or hydrogenolysis) of a wide range of organic substrates. Hence, establishing a realistic adsorption model for hydrogen on nanosized Pt particles as a function of the reaction conditions is of crucial importance to design higher-performing catalysts and/or to correctly choose the operating conditions. Although the first experimental evidence of hydrogen splitting over Pt dates back to the early 1800s,[5,6] and despite the intense research activity by means of both experimental and theoretical approaches, the nature of the Pt-hydrides (i.e., involved Pt adsorption sites) and their relative concentration under different operating conditions are still a matter of discussion.[7,8]

Part of the difficulty is associated with the intrinsic complexity of nanosized noble metal clusters.[9−17] In the last decades a large amount of experimental evidence demonstrated that the Pt clusters undergo electronic and morphological reconstruction as a function of the support, of the adsorbate, and of the reaction temperature.[15,18−26] Pt L_3-edge XAS

Received: May 20, 2019
Published: June 18, 2019

DOI: 10.1021/acscatal.9b02079
ACS Catal. 2019, 9, 7124−7136

spectroscopy (in both XANES and EXAFS regions) has been one of the main techniques employed to investigate the structural and electronic changes experienced by nanometric Pt particles supported on different materials in the presence of hydrogen. As far as the XANES region is concerned, it has been observed that H_2 adsorption on small Pt particles causes dramatic changes in the spectra: the "white line" intensity decreases and the spectra broaden to higher energy as hydrogen is added.[15,20−24,27−35] There have been many efforts to interpret these effects, which are due to both electronic and geometric phenomena.[22,27−42] Most of the analyses are based on subtracting the Pt L_3-edge spectrum of the catalyst in the absence of adsorbed hydrogen (μ(Pt)) from those in the presence of adsorbed hydrogen (μ(Pt−H)), also known as the ΔXANES approach.[43] The resulting difference spectra $\Delta\mu = \mu(\text{Pt−H}) - \mu(\text{Pt})$ contain several features that have been ascribed to specific geometry of the adsorption site on the basis of DFT calculations, although bridged (twofold coordinated) and hollow (threefold coordinated) sites cannot be distinguished.[18,32,35] On the basis of the ΔXANES approach, Koningsberger's group proposed a three-site model for hydrogen adsorption on small Pt particles (coordination number $N_{\text{Pt−Pt}} < 6.5$).[35] The model suggests the presence of three types of hydrides, whose relative concentrations depend on the hydrogen coverage. At very low coverages, hydrogen strongly adsorbs forming linear hydrides, called "atop". At intermediate coverages, due to lateral interactions, the strong "atop" hydrides migrate to *n*-fold coordinated sites (bridged or hollow). If the coverage is increased further, the previously freed "atop" sites are refilled, but this time the interaction is much weaker, giving rise to linear hydrides labeled as "on-top".

As far as the effect of hydrogen adsorption on the Pt L_3-edge EXAFS region is concerned, an elongation of the Pt−Pt first shell distance and a small, but noticeable, increase in the Pt−Pt coordination number upon increasing the amount of hydrogen have been highlighted in many works.[11,20,22,29,30] The former observation was explained by taking into account the electron withdrawing properties of hydrogen, which induces a weakening of the Pt−Pt bond. The increase in the Pt−Pt coordination number was explained in terms of a change of the cluster morphology toward a more spherical shape.

The three-site model was largely improved some years later, by the group of Raybaud and Sautet.[19] The authors simulated, by means of DFT and molecular dynamic calculations, the morphology of a Pt_{13} cluster on γ-Al_2O_3 at increasing hydrogen coverages. In the absence of hydrogen, the Pt cluster is strongly anchored to the γ-Al_2O_3 support with a biplanar morphology. Increasing the hydrogen coverage, linear and *n*-fold coordinated Pt-hydrides are formed, that gradually solvate the Pt_{13} cluster. At the saturation coverage ($Pt_{13}H_{34}$), the cluster assumes a cuboctahedral morphology, largely detached from the support due to the presence of atomic hydrogen at the particle−support interface. Linear and bridge sites are the most favored adsorption modes, and their relative amount is a function of the hydrogen coverage. Similar conclusions were made by Wang and Johnson,[18] on the basis of DFT calculations performed on a carbon-supported Pt_{37} nanoparticle with and without hydrogen passivation. The authors found that a hydrogen atmosphere stabilizes a truncated cuboctahedral morphology, with three (111) and three (100) facets. H atoms prefer to adsorb on bridge sites on the (100) faces and on hollow sites on the (111) ones. When all the bridge and hollow sites are occupied (46 H atoms adsorbed for Pt_{37} clusters), the energy reduction arising from the addition of a further H atom strongly decreases, giving rise to weakly adsorbed linear (on-top) hydrides, in good agreement with the three-site model proposed by Koningsberger.[35] As for the $Pt_{13}H_n$ cluster on γ-Al_2O_3 discussed above, also in this case the Pt-support interaction is reduced significantly with the H passivation, due to the appearance of hydrogen at the interface between the Pt_{37} cluster and the carbon. Both models have the potential to explain most of the experimental evidence reported in the literature.

In such a scenario, a relevant missing detail is the capability of discriminating among several Pt hydrides belonging to the same type. Indeed, there are many reasons to believe that, in a nanometric Pt cluster, the linear Pt-hydrides are not all the same, as well as the bridged or hollow sites differing depending on the environment. For example, up to six different features have been observed in hydrogen TPD curves for polycrystalline Pt,[44−46] suggesting the presence of at least six different adsorption sites characterized by different Pt−H bonding energies. Vibrational spectroscopies might have the capability to discern between different Pt−H species, since the Pt−H vibration is sensitive to even small changes in the coordination geometry. Although some relevant works adopted the IR spectroscopy to investigate the behavior of Pt-supported catalysts in the presence of hydrogen since the early 1960s,[47−52] the use of FT-IR spectroscopy for the direct characterization of the Pt−H species has been largely overlooked, especially in comparison to the huge amount of work based on XAS. This is primarily due to the relatively low dipole moment involved in the Pt−H bond, that reflects into extremely weak ν(Pt−H) absorption bands. The second reason is that in practice only linear Pt−H species can be detected by FT-IR spectroscopy, since the vibrational features of bridged and hollow Pt−H species fall in the region usually obscured by the framework modes of the most employed support materials.[47−50] Incoherent inelastic neutron scattering (INS) might be a powerful alternative, since it is extremely sensitive to hydrogenous species. Indeed, the INS signal is proportional to the neutron cross section of the probed element and to its displacement with respect to the equilibrium position.[53] Hydrogen has the largest incoherent cross section among all the elements and also the largest amplitude of motion because of its lightweight.[53] The use of INS in this field has been limited so far,[54−57] due to the difficulty in having access to the neutron sources, the time required for collecting high-quality data (especially in comparison with X-ray based techniques that in the last decades have seen the rapid development of ultrafast methods), and the large amount of sample necessary for the measurements. Only in recent years the neutron instruments have progressed enough, in terms of neutron flux on the sample and efficiency in the neutron detection, to allow an easier investigation of samples of interest in catalysis.[58]

In this work, we discuss some recent results obtained by coupling INS, FT-IR, and XAS spectroscopies to investigate the dynamic behavior of a highly dispersed Pt/Al_2O_3 catalyst in the presence of hydrogen. At first, we will show that INS and FT-IR spectroscopies may offer a complementary insight into the type and relative abundance of the Pt-hydride species, since INS detects more efficiently *n*-fold coordinated Pt-hydrides while FT-IR spectroscopy discriminates between at least four types of linear Pt−H species, whose relative amount is a function of the hydrogen coverage. In light of this experience,

DOI: 10.1021/acscatal.9b02079
ACS Catal. 2019, 9, 7124−7136

we successively designed a series of DRIFT/XAS/MS experiments aimed at correlating the dynamic behavior of the Pt-hydrides in different reaction conditions with the electronic and structural changes occurring at the Pt nanoparticles. To the best of our knowledge, such an approach was never applied to the study of H_2-induced phenomena occurring on supported Pt nanoparticles.

2. EXPERIMENTAL SECTION

2.1. Catalyst Synthesis and Reduction Procedures. The 5 wt % Pt/Al_2O_3 catalyst was prepared in the Chimet S.p.A. laboratories employing a high-surface-area activated transitional alumina as a support (SSA = 116 m^2 g^{-1}; pore volume = 0.41 cm^3 g^{-1}), and following a deposition−precipitation method similar to the one reported by Kaprielova et al.[59] After preparation, the sample was carefully water washed and dried at 120 °C overnight.

For the INS experiment, Pt/Al_2O_3 (ca. 6.0 g) was activated in dynamic vacuum (final equilibrium pressure P_{eq} = 10^{-4} mbar) at 120 °C and successively reduced in a H_2 atmosphere (two absorption/desorption cycles in hydrogen, absorption pressure: ca. 800 mbar, desorption pressure: dynamic vacuum), at the same temperature for about 1 h, followed by a prolonged evacuation at the same temperature.

For all the *operando* experiments, the catalyst activation and reduction were accomplished following two subsequent steps: (1) the catalyst was heated up to 120 °C (heating rate 5 °C/min) under an inert flow (N_2 or He) and left at this temperature for ca. 30 min, in order to eliminate most of the physisorbed water; (2) the catalyst was treated at 120 °C in a H_2/inert flow for ca. 15 min. During this step, the platinum oxide phase is reduced forming water as a reduction byproduct, followed by formation of Pt-hydrides. We conducted several experiments by changing the total flow rate (in the range 10−50 mL/min) and the H_2 concentration in the gas feed (2, 5, 10 mol %). We found that these two variables do not change the phenomena occurring on the catalyst, but only the involved kinetics (see below).

2.2. Methods. *2.2.1. High Resolution-Transmission Electron Microscopy (HR-TEM).* HR-TEM analysis was performed by means of a JEOL 3010-UHR TEM microscope operating at 300 kV, equipped with a LaB_6 filament, with a 2k × 2k pixels Gatan US1000 CCD camera and with an OXFORD INCA EDS instrument for atomic recognition via energy dispersive spectroscopy. The sample was quickly deposited (in the dry form, i.e., without using any solvent) on a copper grid covered with a lacey carbon film. Histogram of the Pt particle size distribution was obtained by considering a statistical representative number of particles on the HR-TEM images (more than 700), and the mean particle diameter (d_m) was calculated as $\langle d_m \rangle = \frac{\sum d_i n_i}{\sum n_i}$, where n_i is the number of particles of diameter d_i.[16]

2.2.2. Inelastic Neutron Scattering (INS). The INS measurements were performed on the LAGRANGE spectrometer at the ILL facility in Grenoble (France).[60] LAGRANGE is a high resolution filter spectrometer facing an hot moderator allowing the collection of spectra in the 5−525 meV (40−4234 cm^{-1}) energy transfer range with a resolution of $\Delta E/E$ of about 2%. The INS spectra were recorded at 20 K to reduce thermal effects that broaden the spectral features. The raw data are opportunely reduced to the scattering function $S(Q,\omega)$ plotted versus energy transfer (in units of cm^{-1}). The INS spectra were collected in the whole available range, by properly merging the ranges acquired with three different monochromators: Si(111) for the 7.5−20.0 meV range, Si(311) for the 16.0−30.7 meV range, and Cu(220) for the 26.0−525.0 meV range. The integral of the counts of the three data collections in the two overlapped regions has been used to obtain a unified properly normalized spectrum in the whole range.

After activation, a weighed amount of the sample in the powder form was inserted in a volume-calibrated cylindrical-shaped Al cell (4 cm high, 16 mm diameter) within an Ar-filled glovebox to avoid exposure to air. The cell was sealed with an indium-wire, connected to a gas injection stick, and inserted into a CCR cryostat. The Ar contained in the cell was evacuated and the sample was cooled down to 20 K and a first spectrum of the bare activated sample in vacuum was recorded. Successively, the stick was removed from the cryostat and warmed up to room temperature. Hydrogen was dosed at room temperature by means of a Hiden Isochema gas volumetric device, at an equilibrium pressure of 420 mbar. The sample was cooled again at 20 K, and the INS spectrum in the presence of hydrogen was collected.

2.2.3. Operando FT-IR Spectroscopy. For the *operando* FT-IR measurements, ca. 10 mg of the undiluted Pt/Al_2O_3 catalyst were pressed into a self-supported pellet and placed inside a commercial FT-IR reactor cell (AABSPEC, no. 2000-A multimode), which allows recording the FT-IR spectra under controlled temperature and gas atmosphere. The FT-IR spectra were recorded every 60 s during the reduction step, and every 5 min during the successive treatment in N_2 flow. The FT-IR spectra were recorded in transmission mode, at a resolution of 2 cm^{-1}, on a PerkinElmer System 2000 spectrophotometer equipped with a MCT detector.

2.2.4. DRIFT/XAS/MS. *Operando* DRIFT/XAS/MS experiments were carried out at the BM23 beamline[61] of the European Synchrotron Radiation Facility (ESRF, Grenoble, France). Combined diffuse reflectance infrared fourier transform spectroscopy (DRIFT), X-ray absorption spectroscopy (XAS), and mass spectrometry (MS) experiments were performed using a low-volume cell developed at BM23/ID24 for transient experiments.[62] The cell was coupled to a Varian 680 FT-IR spectrophotometer equipped with a high-sensitivity MCT detector.

The Pt/Al_2O_3 catalyst (ca. 5 mg) was loaded in the powder form into a cylindrical channel in the sample holder ca. 1 mm in diameter, with two thin glassy carbon windows to ensure the X-ray beam passing through the sample. The dimension of the channel holder was selected to maximize the quality of the XAS spectra. The sample holder was then placed inside the cell, that was sealed on top with a CaF_2 IR-transparent window. The cell was resistively heated, monitoring the sample temperature by a thermocouple inserted in the cell body. The loaded cell was then mounted into a dedicated infrared optical system designed for DRIFT measurements and connected to the gas line. The outlet was connected to a Balzers Prisma MS via a stainless steel capillary kept at a temperature of 423 K, allowing the detection of a number of pertinent masses at each experiment.

The DRIFT spectra were collected continuously during the XAS measurements, from 900 to 4000 cm^{-1}, at 4 cm^{-1} resolution. Each spectrum (128 scans) required 160 s to be recorded. The spectra were collected in reflectance mode and successively converted into $F(R)$ (Kubelka−Munk). The

DOI: 10.1021/acscatal.9b02079
ACS Catal. 2019, 9, 7124−7136

background was acquired in the same configuration using powdered KBr as a reference.

For Pt L_3-edge XAS, the white beam was monochromatized using a double-crystal Si(111) monochromator, and harmonic rejection was performed using two flat Si mirrors (grazing angle of 2 mrad). The spectra were acquired in transmission using ion chambers for the detection of the reference (I_0) and transmitted (I_t) X-rays. A third ionization chamber recorded a Pt foil reference for energy calibration. The XAS spectra were recorded at the Pt-L_3 edge (11 564 eV) with a beam size of ca. 800 × 100 μm ($H \times V$) through the cell. The energy range was scanned from 11 400 to 12 500 eV, with an energy step of 5 eV and an integration time of 1 s/point in the pre-edge region, 0.5 eV step and 3 s/point in the XANES region, while the step in the EXAFS region was chosen to obtain a 0.04 $Å^{-1}$ step in the k-space with the acquisition time increasing quadratically with k from 3 to 8 s/point. Each spectrum required an acquisition time of about 18 min as a compromise between fast acquisition and quality of the spectra.

2.2.5. XAS Data Analysis. The XANES spectra were aligned and normalized with the Athena software,[63,64] by means of standard procedures. EXAFS data analysis was performed using the Arthemis software.[63,64] The $k^2\chi(k)$ functions were Fourier transformed (FT) in the Δk = 2.6−13.0 $Å^{-1}$ interval. The first-shell fits were performed in the R space (ΔR = 1.0−3.5 Å), resulting in a number of independent parameters $n_{ind} = 2\Delta k \Delta R/\pi$ larger than 16, a value that gives good confidence for a single shell fit.

A preliminary fitting analysis was performed by varying the following parameters: the coordination number (N), the Pt−Pt interatomic distance (R), the correction to the threshold energy (ΔE_0), and the Debye−Waller factor (σ^2). The third-order cumulant, which takes into account the anharmonic correction to the interatomic pair potential, was also included in the analysis, following the indication of previous works.[22,23] The passive electron amplitude reduction factor (S_0^2) was fixed to 0.80(4), as obtained by analyzing the Pt reference foil. The coordination numbers (N) have been obtained by multiplying the amplitude determined by the fit for the first-shell coordination number in platinum bulk (12), and dividing it for the S_0^2 value. Phase and amplitudes were calculated with the FEFF6.0 code[65] using as input the structure of Pt bulk. In order to limit the number of variables, the fit was performed simultaneously on four spectra collected under different H_2 coverage at the same reaction temperature (120 °C). Multiple-scattering paths were not included, since the data analysis was limited to the first coordination shell, and the first-neighbor single-scattering path is well isolated from single- and multiple-scattering paths at longer distance. On the basis of this first analysis, a second series of fits were performed, where the σ^2 was fixed to increasing values from 0.007 to 0.011 $Å^2$, while a single ΔE_0 value was fit across the four H_2 coverages. Advantages and disadvantages of the two fitting strategies are described in more detail in the main text.

3. RESULTS AND DISCUSSION

3.1. Preliminary Characterization of the Pt/Al_2O_3 Catalyst. Figure 1 shows a representative HR-TEM micrograph of Pt/Al_2O_3. Very small Pt nanoparticles, homogeneously distributed on the support, and with an almost spherical shape and a regular size are observed. Most of them have a diameter smaller than 2 nm. The particle size distribution and the average particle size were determined by analyzing more than 700 particles. The estimated average particle size is 1.4 ± 0.4 nm, which is in fair agreement with the nominal dispersion D = 63%, as determined by means of a H_2/O_2 titration method.[66] Such particle size distribution has been demonstrated to be narrow enough to ensure that EXAFS characterization is representative of the whole distribution of particles.[25,26]

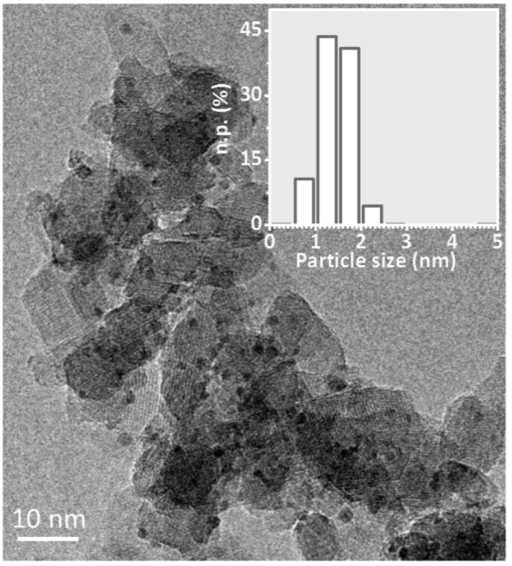

Figure 1. Representative HR-TEM micrograph of Pt/Al_2O_3 and corresponding particle size distribution (inset). Instrumental magnification 200 000×.

3.2. *n*-Fold Coordinated Pt-Hydrides as Detected by Inelastic Neutron Scattering (INS). The Pt/Al_2O_3 system in the presence of H_2 was investigated with the incoherent inelastic neutron scattering (INS) technique. Figure 2a shows the INS spectrum of reduced Pt/Al_2O_3 in the absence (black)

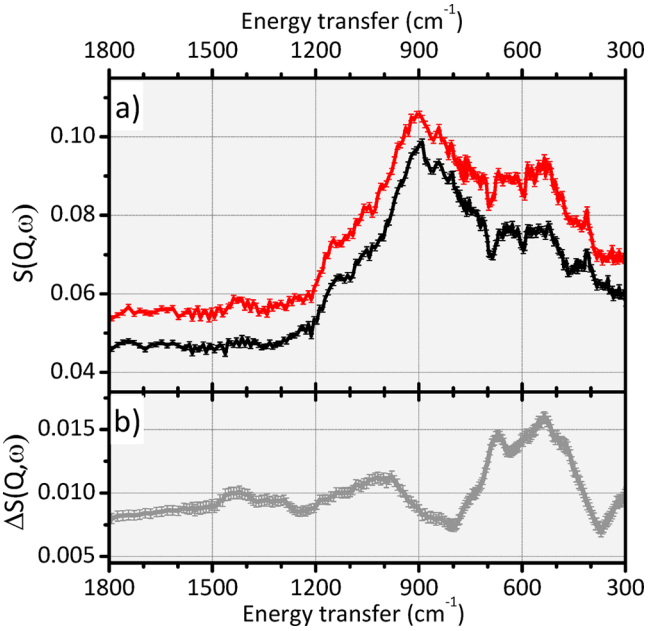

Figure 2. Part (a): INS spectra of the reduced Pt/Al_2O_3 catalyst in the absence (black) and in the presence (red) of 420 mbar of H_2. Part (b): Difference between the two spectra reported in part (a).

DOI: 10.1021/acscatal.9b02079
ACS Catal. 2019, 9, 7124−7136

and in the presence (red) of H_2 (P_{H_2} e.p. = 420 mbar). Both spectra have been collected at 20 K. The two spectra are dominated by an intense peak centered around 905 cm^{-1} (with a shoulder at 760 cm^{-1}) and by a series of overlapping bands at ca. 640 and 550 cm^{-1}, which are all assigned to deformation modes of hydroxyl groups at the alumina surface.[67] Figure 2b shows the difference between the two spectra, $\Delta S(\mathbf{Q},\omega)$, that is the INS spectrum of hydrogen chemisorbed on the catalyst. Indeed, the absence of relevant porosity in the alumina support prevents the observation of physisorbed hydrogen, as reported, for example, for Pt/C catalysts at comparable H_2 equilibrium pressure.[58] The $\Delta S(\mathbf{Q},\omega)$ spectrum is characterized by two series of bands having a broad envelope: (1) the most intense signals are in the range 400−800 cm^{-1} (maxima at 470, 535, 590, 670, 750 cm^{-1}); (2) a second group of bands having medium intensity is observed in the range 800−1200 cm^{-1}. According to the literature,[54,56,57,68,69] all these bands are due to Pt−H vibrations of *n*-fold coordinated (bridged, hollow, and 4-fold coordinated) Pt−H species. Bands in similar positions were previously reported for platinum hydrides on Pt single-crystals,[69] on 40 wt % Pt/C catalysts,[54,56,57] and very recently by some of the authors on a very low loaded, industrially relevant, 5 wt % Pt/C catalyst having a particle size comparable with our Pt/Al_2O_3.[58] The exact assignment of these bands is challenging and would require an accurate modeling of the Pt nanoparticles in the presence of hydrogen, which will be the subject of a successive report. The important message to retain here is that INS clearly reveals the presence of variable *n*-fold coordinated platinum hydrides even in low loaded catalysts.

3.3. Formation of Linear Pt-Hydrides and Their Evolution upon Dehydrogenation, as Monitored by *operando* FT-IR Spectroscopy. A series of preliminary FT-IR measurements during hydrogen adsorption/desorption cycles on Pt/Al_2O_3 were performed using the FT-IR *operando* setup described in the Experimental Section. Figure 3a shows the FT-IR spectra of the catalyst before (black) and after (red) the reduction step. The two spectra are dominated by an intense and very broad absorption band centered at ca. 3500 cm^{-1}, which is due to the ν(OH) of the hydroxyl groups at the alumina surface. Due to the relatively low activation temperature (120 °C), the fraction of the surface OH species is large, and they interact with each other via hydrogen-bonding. The spectra are cut below 1000 cm^{-1}, where the intense vibrational modes of the alumina framework saturate the detector. For this reason, the absorption bands ascribed to *n*-fold coordinated Pt−H species (detected by INS) cannot be detected by means of FT-IR spectroscopy. The spectrum collected at the end of the reduction step (red) shows a small amount of physisorbed H_2O (ν(OH) at ca. 3500 cm^{-1} and δ(HOH) at ca. 1630 cm^{-1}), which derives from the reduction of the supported PtO_x phase, and a series of very weak bands in the 2200−1700 cm^{-1} range. This spectral region is magnified in Figure 3b, that shows the spectra collected during the reduction of the Pt/Al_2O_3 sample after subtraction of the spectrum prior to H_2 dosage. Four absorption bands (labeled ***I***, ***II***, ***III***, and ***IV***) are clearly observable at 2115, 2041, ca. 1990, and ca. 1740 cm^{-1}, respectively. All these bands gradually grow in intensity during the reduction step, and then reach a steady state situation. According to the literature,[47,48,50,51,70] the 2115 cm^{-1} band is attributed to a weak linearly adsorbed hydride, whereas the two bands at 2041 and 1990 cm^{-1} are related to strongly adsorbed linear hydride species. The difference between these two

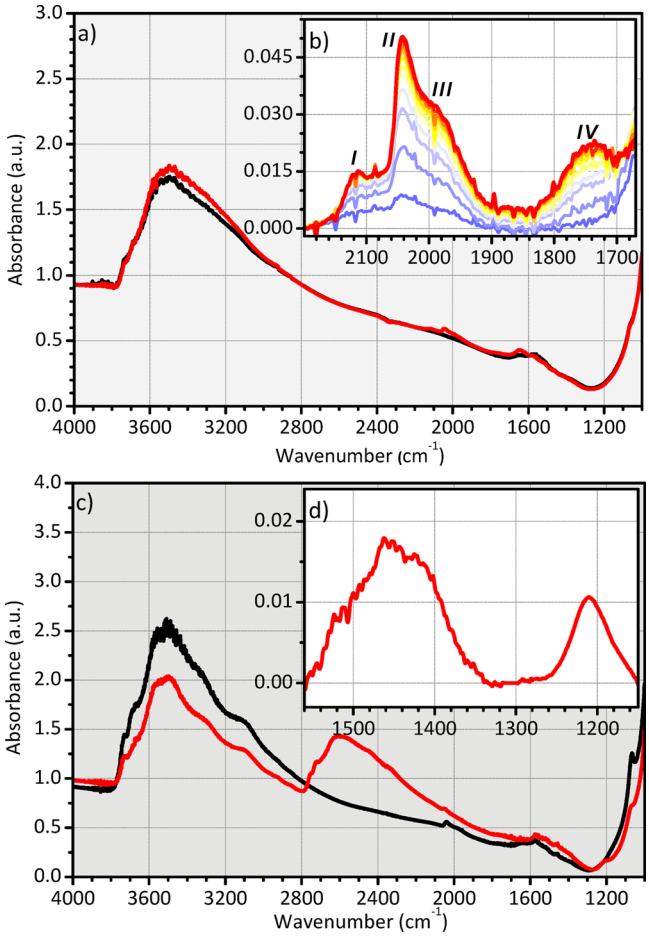

Figure 3. Part (a): FT-IR spectra of the Pt/Al_2O_3 catalyst before (black) and after (red) the reduction step, accomplished in a H_2/N_2 flow (10% H_2, 20 mL/min). Part (b): magnification of the 2200−1700 cm^{-1} range, where linear Pt-hydrides contribute to the spectra. The spectra in part (b) are reported after subtraction of the spectrum prior reduction (black curve in part a). Part (c) FT-IR spectra of the Pt/Al_2O_3 catalyst after the reduction step (black), and the effect of dosing D_2 (red). The spectrum in part (d) is the difference between the two.

strongly adsorbed species was never clarified in the literature, but it might be related to the type of environment around the hydride. A linear hydride strongly adsorbed nearby another hydride (either linear or *n*-fold coordinated) might indeed vibrate differently than an isolated linear one. Finally, the band at ca. 1740 cm^{-1} was never discussed in the literature. We anticipate that it might be assigned to linear platinum hydrides in interaction with the Lewis acid sites exposed at the alumina surface. Hence, this band is strictly correlated with the interface between the platinum nanoparticle and the support.

It is worth noticing that as expected these bands are very weak, because of the rather weak dipole moment associated with the stretching mode of linear Pt−H species. This is the reason why the observation of Pt−H by FT-IR spectroscopy has been limited so far, and often questioned.[49,52] In particular, one of the most frequent criticisms is that the observed bands might be due to chemisorbed CO eventually present as an impurity in the H_2 feed. To be sure that the observed bands are really related to hydride species and not to chemisorbed CO as reported in some cases in the literature,[70] a further experiment was performed by dosing deuterium after the reduction step in

DOI: 10.1021/acscatal.9b02079
ACS Catal. 2019, 9, 7124−7136

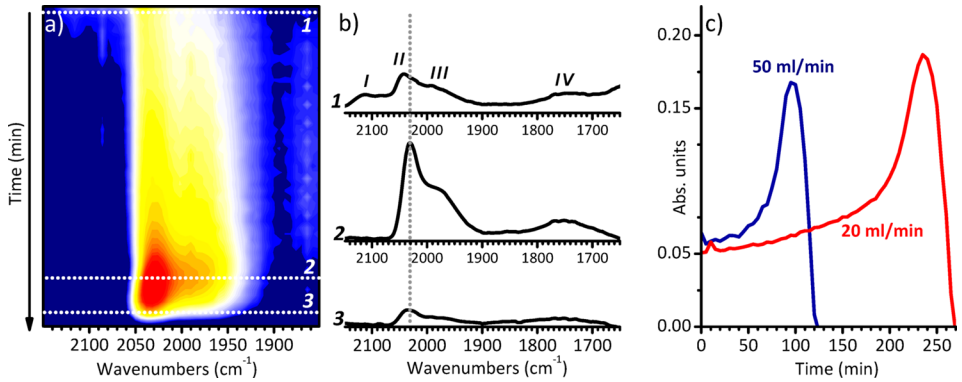

Figure 4. Part (a): 2D map showing the evolution of the FT-IR spectra as a function of time for the Pt/Al_2O_3 catalyst during dehydrogenation in N_2 flow (20 mL/min) at 120 °C. The previous reduction step was accomplished in the presence of 10 mol % H_2 in N_2. The intensity increases from blue to red. Part (b): Three FT-IR spectra selected at specific times (1, 2, and 3 in the 2D map shown in part (a). The four bands are labeled as ***I***, ***II***, ***III***, and ***IV*** (see main text for further discussion). The spectra are shown after subtraction of the spectrum of the catalyst at 120 °C before reduction, in the 2150−1850 cm^{-1} range. Part (c): Evolution of the intensity of the band at 2041 cm^{-1} (species ***II***, dotted vertical line in part b) as a function of time, for the spectra shown in part (a) (20 mL/min, red curve), and for a similar experiment performed with a higher flux (50 mL/min, blue curve).

H_2 (Figure 3c). The FT-IR spectrum of Pt/Al_2O_3 drastically changes, because about half of the surface OH groups undergo exchange with deuterium; hence, the ν(OH) absorption band at ca. 3500 cm^{-1} shifts to 2600 and the δ(OH) band at ca. 1070 cm^{-1} downward shifts to the spectral region dominated by the alumina framework modes. On top of this, four bands are observed at 1515, 1465, 1422, and 1220 cm^{-1} (Figure 3d), corresponding to bands ***I***, ***II***, ***III***, and ***IV*** in Figure 3b. The four bands are isotopically shifted by a factor of ca. 1.39, confirming the assignment to hydride species.[48] The relative intensity of the four bands is slightly different, but this can be due to the change of the profile of the overall spectrum. The Pt−H bands in the 2150−1750 cm^{-1} region do not disappear completely in the presence of D_2, suggesting that the H−D exchange is subjected to a complex equilibrium.

After the reduction step, the gas feed composition was switched to pure N_2 at the constant temperature of 120 °C. Figure 4a shows the evolution of the FT-IR spectra collected in these conditions as a function of time in the form of a 2D map (the intensity increases from blue to red), while Figure 4b shows three selected spectra in the map. The band at 2115 cm^{-1} (species ***I***) immediately disappears, proving that it is associated with a very weakly adsorbed Pt−H species, which is stable only in the presence of a H_2 atmosphere. The other three bands, instead, evolve in a counterintuitive way. In particular, the two bands at 2041 and 1990 cm^{-1} (species ***II*** and ***III***) slowly increase reaching approximately twice their original intensity in about 235 min, while the band at ca. 1740 cm^{-1} (species ***IV***) remains almost unchanged. After reaching the maximum, all the three bands rapidly disappear. Similar experiments were performed by changing the H_2 concentration during the reduction step and/or the total flow rate. The FT-IR spectra evolve in the same way, although with a different velocity. In general, a higher H_2 concentration in the flow caused longer dynamics, while a higher total flow rate was responsible for a shortening. As an example, Figure 4c shows the evolution of the intensity of the band at 2041 cm^{-1} (species ***II***) as a function of time for two experiments performed at the same H_2 concentration (10 mol %) but at a different total flow rate (50 mL/min and 20 mL/min). It is evident that the evolution has the same character, but occurs much faster at 50 mL/min. The reason for these differences has to be ascribed to the experimental setup. Indeed, our *operando* FT-IR cell is characterized by a large dead volume that, once filled with hydrogen during the reduction step, requires time before being completely cleaned by N_2. In other words, our experimental setup allowed a serendipitous decrease of the hydrogen partial pressure in the cell at a very slow speed, thus permitting us to follow the dynamic of the platinum hydrides as a function of the hydrogen coverage.

The evolution of our FT-IR spectra is in very good agreement with the theoretical model proposed by Raybaud and Sautet,[19] according to which a decrease in the hydrogen partial pressure is responsible for a reconstruction of the Pt particles from a cuboctahedral morphology prevalently solvated by *n*-fold coordinated (bridged and hollow) hydrides, to a biplanar morphology mostly covered by linear hydrides. The model predicts that during the reconstruction of the Pt particles, the relative concentration of the linearly adsorbed hydrides (visible by FT-IR spectroscopy) should increase at the expenses of the *n*-fold adsorbed hydrides (which are invisible by FT-IR spectroscopy, but clearly detected by INS, Figure 2). The theoretical model also predicts the existence, in a large range of hydrogen coverages, of hydrogen at the interface between the Pt cluster and the support, corroborating our assignment of the absorption band at ca. 1740 cm^{-1} to platinum hydrides in interaction with alumina. Our FT-IR data fit very well with the simpler three-site model proposed earlier by Koningsberger.[35] At the maximum hydrogen coverage, the Pt particles are covered by adsorbed "on-top" hydrides (species ***I***) and *n*-fold coordinated hydrides (not visible by IR). Upon decreasing the H_2 coverage, the "on-top" hydrides are easily removed and the *n*-fold coordinated hydrides slowly transform themselves into "atop" species, causing the appearance and the transient increase in the intensity of bands ***II*** and ***III***.

3.4. Simultaneous DRIFT/XAS/MS Experiment.

3.4.1. Experimental Results. In order to validate our interpretation, we designed an *ad hoc* DRIFT/XAS/MS experiment to investigate the evolution of the FT-IR bands ascribed to linear Pt-hydrides and, at the same time, the electronic and structural changes occurring at the Pt particles upon decreasing the hydrogen coverage. The main difficulty in coupling DRIFT and XAS spectroscopies in this particular case resides in the unequal time requested for the collection of a

DOI: 10.1021/acscatal.9b02079
ACS Catal. 2019, 9, 7124−7136

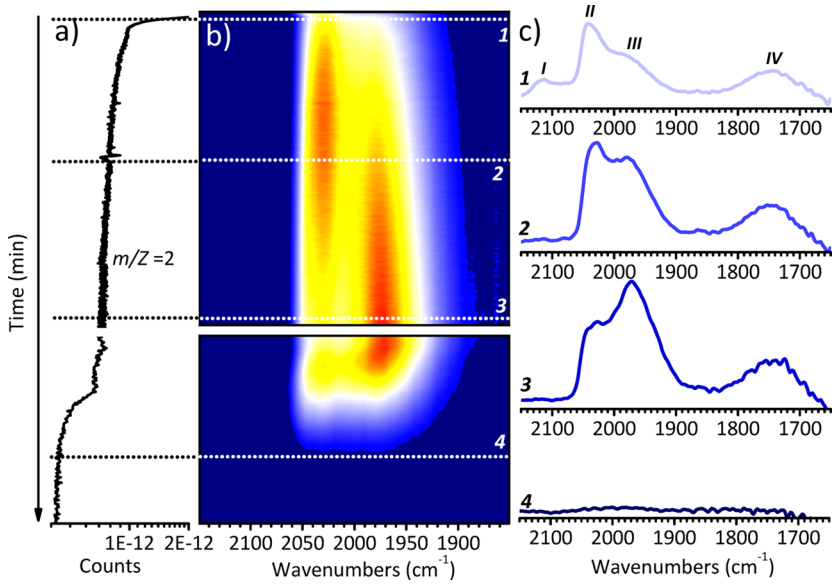

Figure 5. Part (a): Evolution of the signal corresponding to H_2 ($m/Z = 2$) as detected by the mass spectrometer placed at the outlet of the reaction cell. Part (b): 2D map showing the evolution of the DRIFT spectra as a function of time for the Pt/Al_2O_3 catalyst during dehydrogenation in He flow (20 mL/min) at 120 °C, for the operando DRIFT/XAS/MS experiment. The reduction step preceding the dehydrogenation was accomplished in the presence of 10 mol % H_2 in He. The intensity increases from blue to red. Part (c): Four FT-IR spectra selected at specific times (1, 2, 3, and 4 in the 2D map shown in part b). The spectra are shown after subtraction of the spectrum of the catalyst before reduction, in the 2150−1850 cm^{-1} range.

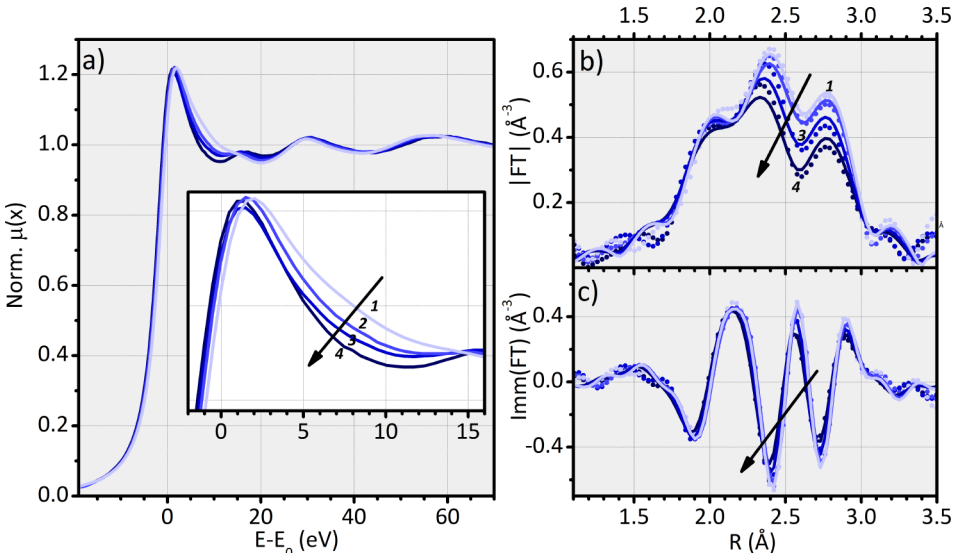

Figure 6. Part (a): Evolution of the normalized Pt L_3-edge XANES spectra of the Pt/Al_2O_3 catalyst during dehydrogenation in He flow (20 mL/min) at 120 °C, collected during the operando DRIFT/XAS/MS experiment (E_0 = 11 564 eV). The inset shows a magnification of the white-line region. Part (b): Modulus of the Fourier-transforms of the k^2-weighted EXAFS signals collected along with the XANES spectra reported in the part a. The experimental signals (dotted) are overlapped to the first shell fits (full line). Part (c): the same as part b, for the imaginary part of the Fourier transforms. Spectra 1−4 closely correspond to the DRIFT spectra 1−4 in Figure 5.

single spectrum: the collection of a good DRIFT spectrum requires around 2 min, while that of a high-quality XAS spectrum in both XANES and EXAFS regions requires 18 min. Thus, it was of pivotal importance to prolong the duration of the hydrogen removal step in order to collect a significant number of good-quality XAS spectra during the Pt particle reconstruction. This problem was overcome by adding to the setup, prior to the measurement cell and tangential to the flow, a dead volume filled with the same hydrogen concentration adopted during the hydride formation step (10 mol %). The dead volume was left open during the dehydrogenation treatment under He flow at 120 °C, so that a tiny and gradually decreasing amount of H_2 was constantly stripped by He. The result was that, after a first sudden drop, the H_2 concentration in the feed decreased very slowly, as detected also by MS at the outlet of the cell (Figure 5a). Only after closure of the dead volume, the H_2 concentration in the feed rapidly fell down to zero (and the m/Z = 2 mass detected by MS reached the end of scale value).

Figure 5b shows the evolution of the DRIFT spectra, in the form of a 2D map, for the Pt/Al_2O_3 catalyst during the dehydrogenation step, whereas Figure 5c shows four selected

DOI: 10.1021/acscatal.9b02079
ACS Catal. 2019, 9, 7124−7136

spectra in the map. The evolution of the absorption bands attributed to linear Pt−H species is even more complex than that observed during the *operando* FT-IR experiments in transmission mode (Figure 4a), likely as a consequence of the longer dynamics. However, the general behavior is the same. Band ***I*** rapidly disappears, while bands ***II*** and ***III*** slowly increase up to double their original intensity, although at a different rate. A change in the relative intensity of bands ***II*** and ***III*** is observed with time, with band ***III*** prevailing at longer dehydrogenation times (i.e., at lower hydrogen concentration). After closing the dead volume, bands ***II*** and ***III*** reach the maximum, and then rapidly disappear. Band ***IV*** is the least affected by the whole dehydrogenation process, and remains almost unchanged in intensity until the end when it disappears swiftly as bands ***II*** and ***III***.

Figure 6 shows the XAS spectra collected simultaneously to the DRIFT and MS spectra previously discussed. The dehydrogenation induces relevant changes in the Pt L_3-edge XANES spectrum of the catalyst (Figure 6a). Both the shape and the intensity of the white line are affected. Specifically, the white line is shifted to lower energy upon decreasing the hydrogen coverage, and becomes sharper (inset in Figure 6a). This is a typical phenomenon that is well-known in the literature, which has been explained mainly in terms of an electronic effect of the adsorbate.[18,22,24,27−30,34−42] Spectrum 4 is collected at the end of the dehydrogenation step and can be considered representative of bare platinum nanoparticles. As far as the EXAFS part of the spectra (Figure 6b,c) is concerned, the dehydrogenation process induces a small but visible decrease in the intensity of the first shell contribution to the FT, and a shift toward shorter distances, which is more visible by looking at the imaginary part of the FT (Figure 6c).

3.4.2. EXAFS Data Analysis. As widely documented in the literature, the EXAFS data analysis of nanometric and subnanometric Pt particles in the presence of adsorbates should be done with caution, since it is difficult to discriminate among the effects of temperature, particle size, and disorder, based on the magnitude of the FT alone.[25,26]

As a first attempt, the fit was performed simultaneously on the four spectra collected under different H_2 coverages at the same temperature (Figure 6b,c), by varying ΔE_0, N, R, σ^2, and the third cumulant. The results are summarized in the first part of Table 1. Without chemisorbed hydrogen (spectrum 4), the Pt−Pt interatomic distance R is 2.70(2) Å. Thus, the Pt−Pt bond is contracted by 0.074 Å compared to bulk Pt (R_{eff} = 2.774 Å), corresponding to ΔR = −2.7%. Contraction values up to 0.10 Å have been reported for particles having similar size.[22,23,71] The mean Pt−Pt bond relaxes in the presence of chemisorbed hydrogen reaching the value R = 2.74(1) Å (ΔR = −1.2%) for spectrum 1. This is also well documented in the literature and is explained in terms of the electron-withdrawing properties of chemisorbed hydrogen, that leads to a reduced electron density among the platinum atoms.[22] The interpretation of the coordination number N and of the Debye−Waller factor σ^2 is more delicate. Without chemisorbed hydrogen (spectrum 4), the Pt nanoparticles are characterized by N = 8.0(8) and σ^2 = 0.0105(9) Å^2. Although these values look reasonable, the trend across the spectral series does not. Indeed, N does not vary within the experimental error and the experimentally observed increase in the amplitude of the FT is all accounted for by σ^2, that drops from 0.0105(9) for spectrum 4 to 0.0085(5) Å^2 for spectrum 1 (i.e., $\Delta\sigma^2$ = −19%). These results are doubtful because the change in σ^2 values

Table 1. Results of the First Shell EXAFS Data Analysis for Spectra 1−4 Reported in Figure 6[a]

First Fitting Approach − R_{factor} = 0.012					
Spectrum	ΔE_0 (eV)	N	R (Å)	σ^2 (Å^2)	σ^3 10^{-4} (Å^3)
1	5.7(6)	8.0(5)	2.738(9)	0.0085(5)	0(1)
2	5.6(5)	7.7(5)	2.717(8)	0.0086(4)	0(1)
3	5.9(9)	8.0(7)	2.71(1)	0.0094(8)	2(2)
4	5.7(9)	8.0(8)	2.70(2)	0.0105(9)	2(2)
Second Fitting Approach − R_{factor} = 0.015					
Spectrum	ΔE_0 (eV)	N	R (Å)	σ^2 (Å^2)	σ^3 10^{-4} (Å^3)
1	5.7(3)	8.4(3)	2.737(7)	0.009	0(1)
2		8.1(2)	2.722(6)		0(1)
3		7.7(4)	2.711(9)		1(1)
4		7.0(4)	2.702(9)		1(2)

[a]The fits were performed simultaneously in the R space (ΔR = 1.0−3.5 Å, Δk = 2.6−13.0 Å^{-1}, resulting in $2\Delta k\Delta R/\pi$ = 16.55), following two approaches. At first, we varied the correction to the threshold energy (ΔE_0), the first shell Pt−Pt coordination number (N), the Pt−Pt interatomic distance (R), the Debye-Waller factor (σ^2), and the third cumulant (σ^3). In a second moment, we fit a single ΔE_0 common to the four spectra, and we fixed σ^2 to increasing values in the 0.007−0.011 Å^2 range. We report here the results of the best fit, obtained for σ^2 = 0.009 Å^2. The results of the other fits are summarized in Figure 7.

looks much larger than expected. In this respect, it is useful to recall that σ^2 contains a static (σ^2_s) and a dynamic (σ^2_d) part, $\sigma^2 = \sigma^2_s + \sigma^2_d$. As demonstrated by Sanchez et al.,[26] the static part σ^2_s depends on both particle size and type of adsorbate. For example, for 1.1 nm Pt nanoparticles (similar to 1.4 nm particles in the current work), σ^2_s was reported to be 0.0045(2) Å^2 in He and 0.0037(2) Å^2 in H_2 atmosphere (extrapolated close to 0 K from $\sigma^2(T)$ curve), indicating that H-passivation induces a strong ordering in the Pt nanoparticles. On the other hand, the dynamic part of the Debye−Waller factor, σ^2_d, depends on both temperature and adsorbate. In particular, it was demonstrated that σ^2_d increases with temperature more rapidly in H_2 than in He.[26] The consequence for Pt nanoparticles is that, although σ^2_s measured in H_2 is lower than that measured in He, for temperatures above a certain threshold the total σ^2 measured in H_2 starts to exceed that measured in He. This threshold is very close to 120 °C for 1.1 nm Pt nanoparticles, meaning that at this temperature the total σ^2 of hydrogenated and bare particles should be very similar to each other. Indeed, from the data of Sanchez et al. the expected difference between the two σ^2 is less than 10^{-4} Å^2, which is well below our fitting error.[26]

The consideration above, and the observation of a very strong correlation between N and σ^2 in our fit, induced us to use another, more conservative, approach in analyzing the EXAFS data, starting from the assumption that for 1.4 nm Pt nanoparticles measured at 120 °C we do not expect σ^2 to vary with any statistical significance with the H_2 concentration. On this basis, we performed a series of fit by varying ΔE_0, N, R, and the third cumulant, and fixing σ^2 at different values in the 0.007−0.011 Å^2 range. The main results are summarized in Figure 7, that shows the behavior of N and R as a function of the H_2 coverage (decreasing from spectrum 1 to spectrum 4), and the R-factor of all the fits. It is evident that the behavior of N and R across the spectral series is the same irrespective of σ^2: N decreases of ca. 20% during the dehydrogenation (from spectrum 1 to spectrum 4), and R decreases of ca. 1.3%.

DOI: 10.1021/acscatal.9b02079
ACS Catal. 2019, 9, 7124−7136

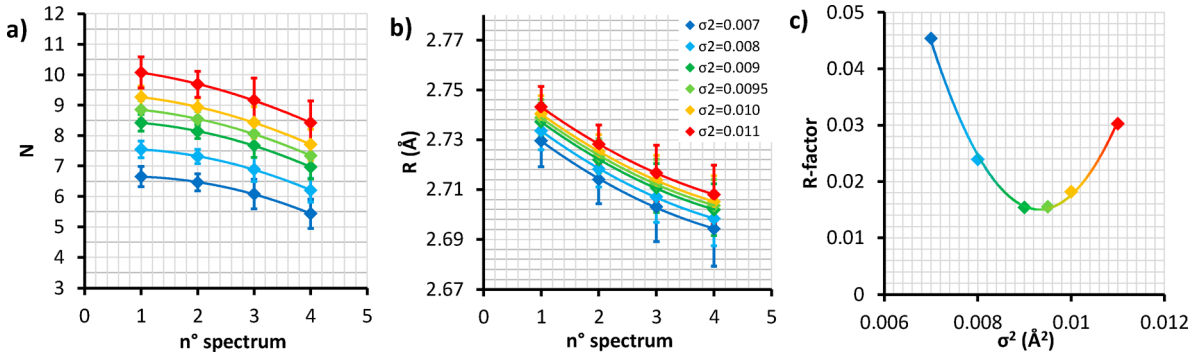

Figure 7. Summary of the results of the EXAFS data analysis on spectra **1**−**4** reported in Figure 6b,c, performed by varying ΔE_0, N, R, and the third cumulant, and fixing σ^2 at different values in the 0.007−0.011 Å^2 range. Parts (a) and (b) show the behavior of N and R across the spectral series, whereas part (c) reports the quality of the fits (R_{factor}) as a function of σ^2.

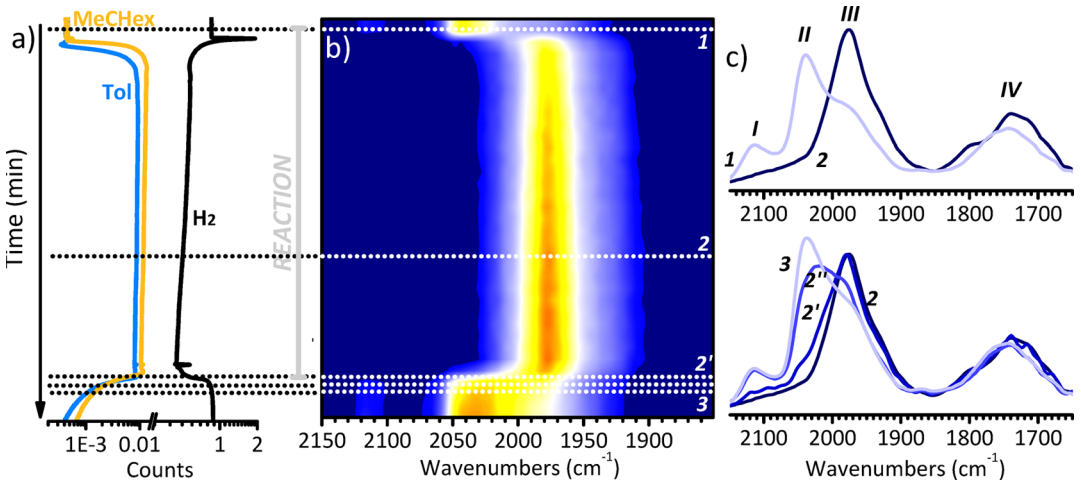

Figure 8. Part (a): Evolution of the signals corresponding to H_2 (m/Z = 2), toluene (m/Z = 91), and methylcyclohexane (m/Z = 55), as detected by the mass spectrometer placed at the outlet of the reaction cell. Part (b): 2D map showing the evolution of the DRIFT spectra as a function of time for the Pt/Al_2O_3 catalyst during hydrogenation of toluene to methylcyclohexane at 120 °C. The reduction step preceding the reaction was accomplished in the presence of 10 mol % H_2 in He. The intensity increases from blue to red. Part (c): FT-IR spectra selected at specific times as indicated in the 2D map shown in part (b). The spectra are shown after subtraction of the spectrum of the catalyst before reduction, in the 2150−1850 cm^{-1} range.

Considering the R_{factor} trend, σ^2 = 0.009 Å^2 is a well-behaved absolute minimum for the fit. The corresponding fitted parameters are reported in the second part of Table 1.

The validity of this approach is testified by the fact that the coordination number N estimated by considering the average particle size as determined by HR-TEM[72,73] and assuming a truncated cuboctahedral model (which is the shape more similar to that expected for dehydrogenated particles)[19] is 7.6, that is just 8% above the N value determined by EXAFS in the absence of H_2.

Overall, the spectroscopic data discussed so far and the detailed EXAFS data analysis clearly demonstrate that the Pt nanoparticles in our Pt/Al_2O_3 catalyst undergo a slow and progressive reconstruction upon hydrogenation/dehydrogenation, in very good agreement with theoretical predictions.[19] XANES and EXAFS techniques were already largely adopted in the past to demonstrate this effect, and our data reproduce those present in the literature. However, the novelty of our work is the simultaneous observation of what happens at the surface of the Pt nanoparticles. The DRIFT spectra collected synchronously to the XAS ones reveal for the first time which kind of platinum hydrides are present at each moment of the dehydrogenation step. Interestingly, species ***IV*** survives for a prolonged time (i.e., also at low hydrogen coverage), suggesting that the platinum hydrides at the Pt/Al_2O_3 interface are quite stable irrespective of the particle morphology. We will see in the following that the observation of what happens at the surface of the Pt nanoparticles will be particularly relevant during the catalysis.

3.5. Behavior of Pt-Hydrides during the Hydrogenation of Toluene. We also investigated the structural and surface dynamics of the Pt nanoparticles in Pt/Al_2O_3 applying the same DRIFT/XAS/MS approach described above, during the catalytic hydrogenation of toluene to methylcyclohexane. The reaction was selected as a model for catalytic hydrogenation of substituted benzenes, because toluene has a high vapor pressure (i.e., it is easily extracted from the liquid phase by an inert flow also at room temperature) and because the IR absorption bands characteristic of reagents and products are clearly discernible and do not overlap with the ν(Pt−H) features we want to monitor. After the reduction step, the 10% H_2 in He flow (20 mL/min) was used to strip toluene vapors from a saturator, and DRIFT/XAS/MS data were collected continuously for ca. 1 h. We selected the aforementioned conditions in order to be far enough from the stoichiometric toluene hydrogenation; in this

DOI: 10.1021/acscatal.9b02079
ACS Catal. 2019, 9, 7124−7136

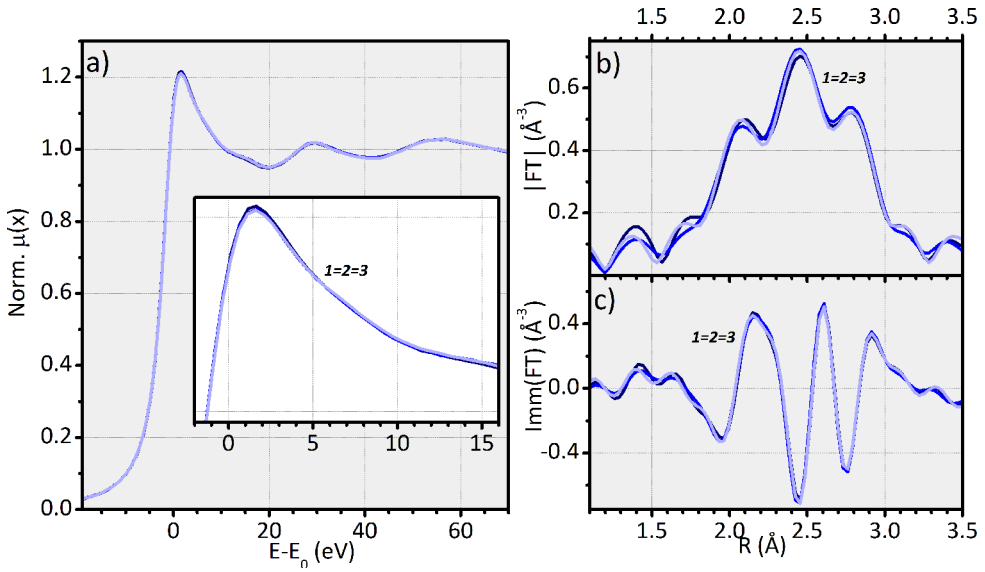

Figure 9. Part (a): Evolution of the normalized Pt L_3-edge XANES spectra of the Pt/Al_2O_3 catalyst during hydrogenation of toluene to methylcyclohexane at 120 °C, collected during the operando DRIFT/XAS/MS experiment (E_0 = 11 564 eV). The inset shows a magnification of the white-line region. Part (b): Modulus of the Fourier-transforms of the k^2-weighted EXAFS signals collected along with the XANES spectra reported in part a. Part (c): the same as part b, for the imaginary part of the Fourier Transforms. Spectra **1**−**3** closely correspond to the DRIFT spectra **1**−**3** in Figure 8 (i.e., spectrum **1** is collected before introducing toluene in the reaction feed, spectrum **2** during the toluene hydrogenation reaction, and spectrum **3** after removal of toluene from the reaction feed).

way, we are sure to avoid the total depletion of the Pt-hydride species that we are interested in during the reaction. The DRIFT and MS results are summarized in Figure 8, while the XANES and EXAFS results are shown in Figure 9.

The MS data (Figure 8a) indicate that toluene conversion starts instantaneously and proceeds at a constant rate for the whole investigated time. At the same time, relevant changes are observed in the DRIFT spectra (Figure 8b,c): bands ***I*** and ***II*** immediately disappear, while band ***III*** rapidly increases in intensity. In contrast, band ***IV*** is almost unaffected. The spectra remain then constant along the whole reaction. The reverse behavior is observed when, after ca. 1 h of reaction, toluene is removed from the reaction feed. Band ***III*** decreases in intensity, and bands ***II*** and ***I*** are restored again. The spectrum collected in these conditions (spectrum 3) is almost equal to that collected before the onset of the reaction (spectrum 1). Interestingly, no changes are observed neither in the XANES spectra (Figure 9a) nor in the EXAFS ones along all the reaction time (Figure 9b,c). This univocally demonstrates that, in the adopted experimental conditions, the Pt nanoparticles are structurally and electronically stable during the whole reaction time.

Taken as a whole, these results indicate that, under the adopted experimental conditions, the changes occurring at the Pt surface during the catalysis are not accompanied by a change in the structure and morphology of the Pt nanoparticles. Moreover, the DRIFT data shown in Figure 8b,c suggest that only a fraction of the platinum hydrides are directly involved in the hydrogenation reaction. Species ***I***, which are the weakly adsorbed hydrides (hence more available), are immediately consumed and no longer observed during the reaction, a behavior that indicates their direct participation in the reaction. The destiny of species ***II*** is less straightforward. Indeed, band ***II*** also immediately disappears as soon as toluene reaches the sample. However, a careful inspection to the sequence of the spectra suggests that it is converted into band ***III***. Indeed, an isosbestic point is observed at 2006 cm^{-1}. Hence, in the presence of toluene, the strongly adsorbed hydrides of type ***II*** are converted into hydrides of type ***III***. This is the same effect observed during the dehydrogenation, when band ***III*** increases in intensity at the expense of band ***II*** (Figure 5b,c). This evidence further corroborates the assignment of bands ***II*** and ***III*** to very similar strongly adsorbed "atop" platinum hydrides that differ in terms of the surface environment. Species ***III*** is more isolated than species ***II***, and hence is favored in the presence of toluene, that competes for the adsorbing sites at the platinum surface. Finally, species ***IV*** seems unaffected by the occurrence of the reaction, as also observed during the dehydrogenation. Even though the majority of the observed linear Pt-hydrides do not participate directly to the hydrogenation reaction (i.e., they are not used to hydrogenate the substrate), they play a fundamental role, maintaining the Pt nanoparticle shape along the reaction.

4. CONCLUSIONS

It is a well-known phenomenon that supported Pt nanoparticles subjected to hydrogenation conditions undergo electronic and morphological reconstructions depending on a range of parameters, among which are the employed support, the adopted temperature and pressure, the atmospheric composition, and the hydrogen coverage. So far, the occurrence of these reconstruction phenomena has been predicted by theoretical calculation on different Pt-based systems,[18,19,35] which are in good agreement with the structural and electronic information derived from EXAFS and XANES data. However, a complete experimental characterization of all the surface Pt-hydride species and of their dynamic behavior in different reaction conditions was still missing, despite its crucial importance in hydrogenation catalysis. In this work we have tried to fill this gap, by investigating an industrial 5 wt % Pt/Al_2O_3 catalyst (average particle size of 1.4 ± 0.4 nm) under

DOI: 10.1021/acscatal.9b02079
ACS Catal. 2019, 9, 7124−7136

different hydrogenation/dehydrogenation conditions with a multitechniques approach, including HR-TEM, INS and FT-IR spectroscopy, and synchronous DRIFT/XAS/MS.

Briefly, we have been able to identify at the Pt surface both *n*-fold coordinated Pt-hydrides and four different types of linear Pt-hydrides characterized by different adsorption strengths. We have observed experimentally the conversion of the *n*-fold coordinated hydrides into linear ones upon decreasing the hydrogen coverage, and vice versa, and correlated it to the morphological and electronic reconstruction of the Pt nanoparticles, in fair agreement with the theoretical predictions.[19] Even more important for the catalysis, we have demonstrated that only the weakest adsorbed hydrides (species ***I***) are directly involved in the hydrogenation of toluene (chosen as a model hydrogenation reaction). All the other surface hydrides, however, play an indirect but fundamental role, since they maintain the Pt nanoparticles H-solvated, and hence electronically and morphologically stable during the reaction, avoiding the occurrence of deactivation processes.

From a more general point of view, the data shown in this work clearly reveal how the catalytic phenomena occurring at metal nanoparticles arise from a delicate balance of electronic, geometric, and surface properties. Understanding how to optimize all these features is of extreme importance to design increasingly performing catalysts, but it requires the concerted application of several complementary characterization techniques. In this respect, we wish to emphasize that each technique employed in this work, if taken as a single measurement, cannot lead to a complete picture of the whole problem. For example, XAS spectroscopy is not able to distinguish the surface Pt-hydride species directly involved in catalysis, while FT-IR and INS spectroscopies detect only a fraction of the surface Pt−H species and are unable to determine the structure and morphology of the Pt nanoparticles.

AUTHOR INFORMATION

Corresponding Author

*E-mail: elena.groppo@unito.it.

ORCID

Andrea Lazzarini: 0000-0002-0404-6597
Sara Morandi: 0000-0003-0577-7911
Maela Manzoli: 0000-0002-4427-7939
Kirill A. Lomachenko: 0000-0003-0238-1719
Monica Jimenez Ruiz: 0000-0002-9856-807X
Carlo Lamberti: 0000-0001-8004-2312
Andrea Piovano: 0000-0002-5005-6307
Elena Groppo: 0000-0003-4153-5709

Notes

The authors declare no competing financial interest.

REFERENCES

(1) Blaser, H.-U.; Schnyder, A.; Steiner, H.; Roessler, F.; Baumeister, P., Selective hydrogenation of functionalized hydrocarbons. In *Handbook of Heterogeneous Catalysis*, 2nd ed., Ertl, G.; Knoezinger, H.; Schuth, F.; Weitkamp, J., Eds.; Wiley-VCH Verlag GmbH & Co. KGaA, 2008; Vol. *1*, pp 3284−3308.

(2) Ertl, G.; Knoezinger, H., Eds. *Handbook of Heterogeneous Catalysis*; Wiley-VCH, 1997; Vol. *5*.

(3) Nishimura, S. *Handbook of Heterogeneous Catalytic Hydrogenation for Organic Synthesis*; Wiley, 2001.

(4) Rylander, P. *Catalytic Hydrogenation in Organic Syntheses*; Academic Press, 1979.

(5) Che, M. Nobel Prize in chemistry 1912 to Sabatier: Organic chemistry or catalysis? *Catal. Today* **2013**, *218−219*, 162−171.

(6) Zecchina, A.; Califano, S. Chapter 1 - From the Onset to the First Large-Scale Industrial Processes. In *The Development of Catalysis: A History of Key Processes and Personas in Catalytic Science and Technology*; John Wiley & Sons, 2017; pp 1−57.

(7) Andrews, L.; Wang, X.; Manceron, L. Infrared spectra and density functional calculations of platinum hydrides. *J. Chem. Phys.* **2001**, *114*, 1559−1566.

(8) Mueller, W. M.; Blackledge, J. P.; Libowitz, G. G. *Metal Hydrides*; Academic, 1968.

(9) Beale, A. M.; Sankar, G. Following the structural changes in iron phosphate catalysts by in situ combined XRD/QuEXAFS technique. *J. Mater. Chem.* **2002**, *12*, 3064−3072.

(10) Brueckner, A. Simultaneous combination of in situ-EPR/UV-VIS/on line GC: a novel setup for investigating transition metal oxide catalysts under working conditions. *Chem. Commun. (Cambridge, U. K.)* **2001**, 2122−2123.

(11) Frenkel, A. I.; Small, M. W.; Smith, J. G.; Nuzzo, R. G.; Kvashnina, K. O.; Tromp, M. An in Situ Study of Bond Strains in 1 nm Pt Catalysts and Their Sensitivities to Cluster-Support and Cluster-Adsorbate Interactions. *J. Phys. Chem. C* **2013**, *117*, 23286−23294.

(12) Grunwaldt, J.-D.; Clausen, B. S. Combining XRD and EXAFS with on-Line Catalytic Studies for in situ Characterization of Catalysts. *Top. Catal.* **2002**, *18*, 37−43.

(13) Marinkovic, N. S.; Wang, Q.; Frenkel, A. I. In situ diffuse reflectance IR spectroscopy and X-ray absorption spectroscopy for fast catalytic processes. *J. Synchrotron Radiat.* **2011**, *18*, 447−455.

(14) Newton, M. A.; Jyoti, B.; Dent, A. J.; Fiddy, S. G.; Evans, J. Synchronous, time resolved, diffuse reflectance FT-IR, energy dispersive EXAFS (EDE) and mass spectrometric investigation of the behaviour of Rh catalysts during NO reduction by CO. *Chem. Commun. (Cambridge, U. K.)* **2004**, 2382−2383.

(15) Small, M. W.; Sanchez, S. I.; Marinkovic, N. S.; Frenkel, A. I.; Nuzzo, R. G. Influence of Adsorbates on the Electronic Structure, Bond Strain, and Thermal Properties of an Alumina-Supported Pt Catalyst. *ACS Nano* **2012**, *6*, 5583−5595.

(16) Agostini, G.; Pellegrini, R.; Leofanti, G.; Bertinetti, L.; Bertarione, S.; Groppo, E.; Zecchina, A.; Lamberti, C. Determination of the Particle Size, Available Surface Area, and Nature of Exposed Sites for Silica-Alumina-Supported Pd Nanoparticles: A Multi-technical Approach. *J. Phys. Chem. C* **2009**, *113*, 10485−10492.

(17) Arrigo, R.; Badmus, K.; Baletto, F.; Boeije, M.; Bowker, M.; Brinkert, K.; Bugaev, A.; Bukhtiyarov, V.; Carosso, M.; Catlow, R.; Chanerika, R.; Davies, P. R.; Dononelli, W.; Freund, H. J.; Friend, C.; Gallarati, S.; Gates, B.; Genest, A.; Gibson, E. K.; Hargreaves, J.; Helveg, S.; Huang, H.; Hutchings, G.; Irvine, N.; Johnston, R.; Lai, S.; Lamberti, C.; Macginley, J.; Marchant, D.; Murayama, T.; Nome, R.; Odarchenko, Y.; Quinson, J.; Rogers, S.; Russell, A.; Said, S.; Sermon, P.; Shah, P.; Simoncelli, S.; Soulantica, K.; Spolaore, F.; Tooze, B.; Torrente-Murciano, L.; Trunschke, A.; Willock, D.; Zhang, J. The challenges of characterising nanoparticulate catalysts: General discussion. *Faraday Discuss.* **2018**, *208*, 339−394.

(18) Wang, L.-L.; Johnson, D. D. Shear Instabilities in Metallic Nanoparticles: Hydrogen-Stabilized Structure of Pt37 on Carbon. *J. Am. Chem. Soc.* **2007**, *129*, 3658−3664.

(19) Mager-Maury, C.; Bonnard, G.; Chizallet, C.; Sautet, P.; Raybaud, P. H2-induced reconstruction of supported Pt clusters: metal-support interaction versus surface hydride. *ChemCatChem* **2011**, *3*, 200−207.

(20) Alexeev, O. S.; Li, F.; Amiridis, M. D.; Gates, B. C. Effects of Adsorbates on Supported Platinum and Iridium Clusters: Characterization in Reactive Atmospheres and during Alkene Hydrogenation Catalysis by X-ray Absorption Spectroscopy. *J. Phys. Chem. B* **2005**, *109*, 2338−2349.

DOI: 10.1021/acscatal.9b02079
ACS Catal. 2019, 9, 7124−7136

(21) Kang, J. H.; Menard, L. D.; Nuzzo, R. G.; Frenkel, A. I. Unusual Non-Bulk Properties in Nanoscale Materials: Thermal Metal-Metal Bond Contraction of γ-Alumina-Supported Pt Catalysts. *J. Am. Chem. Soc.* **2006**, *128*, 12068−12069.
(22) Bus, E.; van Bokhoven, J. A. Hydrogen chemisorption on supported platinum, gold, and platinum-gold-alloy catalysts. *Phys. Chem. Chem. Phys.* **2007**, *9*, 2894−2902.
(23) Bus, E.; Miller, J. T.; Kropf, A. J.; Prins, R.; van Bokhoven, J. A. Analysis of in situ EXAFS data of supported metal catalysts using the third and fourth cumulant. *Phys. Chem. Chem. Phys.* **2006**, *8*, 3248−3258.
(24) Bus, E.; Miller, J. T.; van Bokhoven, J. A. Hydrogen chemisorption on Al2O3-supported gold catalysts. *J. Phys. Chem. B* **2005**, *109*, 14581−14587.
(25) Li, L.; Wang, L.-L.; Johnson, D. D.; Zhang, Z.; Sanchez, S. I.; Kang, J. H.; Nuzzo, R. G.; Wang, Q.; Frenkel, A. I.; Li, J.; Ciston, J.; Stach, E. A.; Yang, J. C. Noncrystalline-to-Crystalline Transformations in Pt Nanoparticles. *J. Am. Chem. Soc.* **2013**, *135*, 13062−13072.
(26) Sanchez, S. I.; Menard, L. D.; Bram, A.; Kang, J. H.; Small, M. W.; Nuzzo, R. G.; Frenkel, A. I. The Emergence of Nonbulk Properties in Supported Metal Clusters: Negative Thermal Expansion and Atomic Disorder in Pt Nanoclusters Supported on γ-Al2O3. *J. Am. Chem. Soc.* **2009**, *131*, 7040−7054.
(27) Lytle, F. W.; Wei, P. S. P.; Greegor, R. B.; Via, G. H.; Sinfelt, J. H. Effect of chemical environment on magnitude of x-ray absorption resonance at LIII edges. Studies on metallic elements, compounds, and catalysts. *J. Chem. Phys.* **1979**, *70*, 4849−4855.
(28) Vaarkamp, M.; Miller, J. T.; Modica, F. S.; Koningsberger, D. C. On the relation between particle morphology, structure of the metal-support interface, and catalytic properties of Pt/γ-Al2O3. *J. Catal.* **1996**, *163*, 294−305.
(29) Reifsnyder, S. N.; Otten, M. M.; Sayers, D. E.; Lamb, H. H. Hydrogen Chemisorption on Silica-Supported Pt Clusters: In Situ X-ray Absorption Spectroscopy. *J. Phys. Chem. B* **1997**, *101*, 4972−4977.
(30) Ramaker, D. E.; Mojet, B. L.; Garriga Oostenbrink, M. T.; Miller, J. T.; Koningsberger, D. C. Contribution of shape resonance and Pt-H EXAFS in the Pt L2,3 X-ray absorption edges of supported Pt particles: Application and consequences for catalyst characterization. *Phys. Chem. Chem. Phys.* **1999**, *1*, 2293−2302.
(31) Ankudinov, A. L.; Rehr, J. J.; Low, J. J.; Bare, S. R. Theoretical interpretation of XAFS and XANES in Pt clusters. *Top. Catal.* **2002**, *18*, 3−7.
(32) Ankudinov, A. L.; Rehr, J. J.; Low, J. J.; Bare, S. R. Effect of hydrogen adsorption on the x-ray absorption spectra of small Pt clusters. Reply to Comment. *Phys. Rev. Lett.* **2002**, *89*, 139702−139701.
(33) Koningsberger, D. C.; Oudenhuijzen, M. K.; De Graaf, J.; Van Bokhoven, J. A.; Ramaker, D. E. In situ X-ray absorption spectroscopy as a unique tool for obtaining information on hydrogen binding sites and electronic structure of supported Pt catalysts: towards an understanding of the compensation relation in alkane hydrogenolysis. *J. Catal.* **2003**, *216*, 178−191.
(34) Teliska, M.; O'Grady, W. E.; Ramaker, D. E. Determination of H Adsorption Sites on Pt/C Electrodes in HClO4 from Pt L2,3 X-ray Absorption Spectroscopy. *J. Phys. Chem. B* **2004**, *108*, 2333−2344.
(35) Oudenhuijzen, M. K.; Van Bokhoven, J. A.; Miller, J. T.; Ramaker, D. E.; Koningsberger, D. C. Three-Site Model for Hydrogen Adsorption on Supported Platinum Particles: Influence of Support Ionicity and Particle Size on the Hydrogen Coverage. *J. Am. Chem. Soc.* **2005**, *127*, 1530−1540.
(36) Asakura, K.; Kubota, T.; Ichikuni, N.; Iwasawa, Y. A new characterization method for adsorbed hydrogen on supported Pt particles. *Stud. Surf. Sci. Catal.* **1996**, *101*, 911−919.
(37) Ichikuni, N.; Iwasawa, Y. In situ d electron density of platinum particles on supports by XANES. *Catal. Lett.* **1993**, *20*, 87−95.
(38) Kubota, T.; Asakura, K.; Ichikuni, N.; Iwasawa, Y. A new method for quantitative characterization of adsorbed hydrogen on Pt particles by means of Pt L-edge XANES. *Chem. Phys. Lett.* **1996**, *256*, 445−448.
(39) Mansour, A. N.; Cook, J. W., Jr.; Sayers, D. E. Quantitative technique for the determination of the number of unoccupied d-electron states in a platinum catalyst using the L2,3 x-ray absorption edge spectra. *J. Phys. Chem.* **1984**, *88*, 2330−2334.
(40) Mojet, B. L.; Miller, J. T.; Ramaker, D. E.; Koningsberger, D. C. A New Model Describing the Metal-Support Interaction in Noble Metal Catalysts. *J. Catal.* **1999**, *186*, 373−386.
(41) Samant, M. G.; Boudart, M. Support effects on electronic structure of platinum clusters in Y zeolite. *J. Phys. Chem.* **1991**, *95*, 4070−4074.
(42) Watari, N.; Ohnishi, S. Electronic structure of H adsorbed on Pt13 clusters. *J. Chem. Phys.* **1997**, *106*, 7531−7540.
(43) Ramaker, D. E., Novel XAS Techniques for Probing Fuel Cells and Batteries. In *X-Ray Absorption and X-Ray Emission Spectroscopy: Theory and Applications*, van Bokhoven, J. A.; Lamberti, C., Eds.; John Wiley & Sons: Chichester (UK), 2016; pp 485−522.
(44) Tsuchiya, S.; Amenomiya, Y.; Cvetanovic, R. J. Study of metal catalysts by temperature programmed desorption. II. Chemisorption of hydrogen on platinum. *J. Catal.* **1970**, *19*, 245−255.
(45) Dixon, L. T.; Barth, R.; Kokes, R. J.; Gryder, J. W. Hydrogen adsorption by alumina-supported platinum. *J. Catal.* **1975**, *37*, 376−382.
(46) Miller, J. T.; Meyers, B. L.; Modica, F. S.; Lane, G. S.; Vaarkamp, M.; Koningsberger, D. C. Hydrogen temperature-programmed desorption (H2 TPD) of supported platinum catalysts. *J. Catal.* **1993**, *143*, 395−408.
(47) Pliskin, W. A.; Eischens, R. P. Infrared spectra of hydrogen and deuterium chemisorbed on platinum. *Z. Phys. Chem. (Muenchen, Ger.)* **1960**, *24*, 11−23.
(48) Eley, D. D.; Moran, D. M.; Rochester, C. H. Infrared study of interaction between hydrogen and supported platinum catalysts. *Trans. Faraday Soc.* **1968**, *64*, 2168−2180.
(49) Primet, M.; Basset, J. M.; Mathieu, M. V.; Prettre, M. Infrared investigation of hydrogen adsorption on alumina-supported platinum. *J. Catal.* **1973**, *28*, 368−375.
(50) Dixon, L. T.; Barth, R.; Gryder, J. W. Infrared active species of hydrogen adsorbed by alumina-supported platinum. *J. Catal.* **1975**, *37*, 368−375.
(51) Candy, J. P.; Fouilloux, P.; Primet, M. Hydrogen adsorption between 300 and 873 K on a platinum/magnesium oxide catalyst. *Surf. Sci.* **1978**, *72*, 167−176.
(52) Szilagyi, T. Fourier-transform infrared study of weak adsorption of hydrogen on platinum/silica. *J. Catal.* **1990**, *121*, 223−227.
(53) Mitchell, P. C. H.; Parker, S. F.; Ramirez-Cuesta, A. J.; Tomkinson, J. *Vibrational Spectroscopy With Neutrons, With Applications in Chemistry, Biology, Materials Science and Catalysis*; World Scientific: Singapore, 2005.
(54) Albers, P.; Auer, E.; Ruth, K.; Parker, S. F. Inelastic Neutron Scattering Investigation of the Nature of Surface Sites Occupied by Hydrogen on Highly Dispersed Platinum on Commercial Carbon Black Supports. *J. Catal.* **2000**, *196*, 174−179.
(55) Albers, P. W.; Krauter, J. G. E.; Ross, D. K.; Heidenreich, R. G.; Koehler, K.; Parker, S. F. Identification of Surface States on Finely Divided Supported Palladium Catalysts by Means of Inelastic Incoherent Neutron Scattering. *Langmuir* **2004**, *20*, 8254−8260.
(56) Albers, P. W.; Lopez, M.; Sextl, G.; Jeske, G.; Parker, S. F. Inelastic neutron scattering investigation on the site occupation of atomic hydrogen on platinum particles of different size. *J. Catal.* **2004**, *223*, 44−53.
(57) Parker, S. F.; Frost, C. D.; Telling, M.; Albers, P.; Lopez, M.; Seitz, K. Characterisation of the adsorption sites of hydrogen on Pt/C fuel cell catalysts. *Catal. Today* **2006**, *114*, 418−421.
(58) Carosso, M.; Lazzarini, A.; Piovano, A.; Pellegrini, R.; Morandi, S.; Manzoli, M.; Vitillo, J. G.; Ruiz, M. J.; Lamberti, C.; Groppo, E. Looking for the active hydrogen species in a 5 wt% Pt/C catalyst: a challenge for inelastic neutron scattering. *Faraday Discuss.* **2018**, *208*, 227−242.
(59) Kaprielova, K. M.; Yakovina, O. A.; Ovchinnikov, I. I.; Koscheev, S. V.; Lisitsyn, A. S. Preparation of platinum-on-carbon

DOI: 10.1021/acscatal.9b02079
ACS Catal. 2019, 9, 7124−7136

catalysts via hydrolytic deposition: Factors influencing the deposition and catalytic properties. *Appl. Catal., A* **2012**, *449*, 203−214.
(60) Piovano, A.; Agostini, G.; Carosso, M.; Groppo, E.; Jimenez Ruiz, M.; Lamberti, C.; Lazzarini, A.; Manzoli, M.; Morandi, S.; Pellegrini, R.; Vottero, E. *Study of the Pt-hydride formation and spillover effect on Pt/Al_2O_3 and Pt/C catalysts*; 2016; DOI: 10.5291/ILL-DATA.7-05-466.
(61) Mathon, O.; Beteva, A.; Borrel, J.; Bugnazet, D.; Gatla, S.; Hino, R.; Kantor, I.; Mairs, T.; Munoz, M.; Pasternak, S.; Perrin, F.; Pascarelli, S. The time-resolved and extreme conditions XAS (Texas) facility at the European Synchrotron Radiation Facility: The general-purpose EXAFS bending-magnet beamline BM23. *J. Synchrotron Radiat.* **2015**, *22*, 1548−1554.
(62) Agostini, G.; Meira, D.; Monte, M.; Vitoux, H.; Iglesias-Juez, A.; Fernandez-Garcia, M.; Mathon, O.; Meunier, F.; Berruyer, G.; Perrin, F.; Pasternak, S.; Mairs, T.; Pascarelli, S.; Gorges, B. XAS/DRIFTS/MS spectroscopy for time-resolved operando investigations at high temperature. *J. Synchrotron Radiat.* **2018**, *25*, 1745−1752.
(63) Newville, M. IFEFFIT: interactive XAFS analysis and FEFF fitting. *J. Synchrotron Radiat.* **2001**, *8*, 322−324.
(64) Ravel, B.; Newville, M. ATHENA, ARTEMIS, HEPHAESTUS: data analysis for X-ray absorption spectroscopy using IFEFFIT. *J. Synchrotron Radiat.* **2005**, *12*, 537−541.
(65) Zabinsky, S. I.; Rehr, J. J.; Ankudinov, A.; Albers, R. C.; Eller, M. J. Multiple-Scattering Calculations of X-Ray-Absorption Spectra. *Phys. Rev. B: Condens. Matter Mater. Phys.* **1995**, *52*, 2995−3009.
(66) Benson, J. E.; Boudart, M. Hydrogen-oxygen titration method for the measurement of supported platinum surface areas. *J. Catal.* **1965**, *4*, 704−710.
(67) McInroy, A. R.; Lundie, D. T.; Winfield, J. M.; Dudman, C. C.; Jones, P.; Parker, S. F.; Lennon, D. The interaction of alumina with HCl: An infrared spectroscopy, temperature-programmed desorption and inelastic neutron scattering study. *Catal. Today* **2006**, *114*, 403−411.
(68) Kolesnikov, A. I.; Antonov, V. E.; Bashkin, I. O.; Grosse, G.; Moravsky, A. P.; Muzychka, A. Y.; Ponyatovsky, E. G.; Wagner, F. E. Neutron spectroscopy of C60 fullerene hydrogenated under high pressure; evidence for interstitial molecular hydrogen. *J. Phys.: Condens. Matter* **1997**, *9*, 2831−2838.
(69) Renouprez, A. J.; Jobic, H. Neutron scattering study of hydrogen adsorption on platinum catalysts. *J. Catal.* **1988**, *113*, 509−516.
(70) Paleček, D.; Tek, G.; Lan, J.; Iannuzzi, M.; Hamm, P. Characterization of the Platinum−Hydrogen Bond by Surface-Sensitive Time-Resolved Infrared Spectroscopy. *J. Phys. Chem. Lett.* **2018**, *9*, 1254−1259.
(71) Delley, B.; Ellis, D. E.; Freeman, A. J.; Baerends, E. J.; Post, D. Binding energy and electronic structure of small copper particles. *Phys. Rev. B: Condens. Matter Mater. Phys.* **1983**, *27*, 2132−2144.
(72) Agostini, G.; Piovano, A.; Bertinetti, L.; Pellegrini, R.; Leofanti, G.; Groppo, E.; Lamberti, C. Effect of different face centered cubic nanoparticle distributions on particle size and surface area determination: A theoretical study. *J. Phys. Chem. C* **2014**, *118*, 4085−4094.
(73) Montejano-Carrizales, J. M.; Aguilera-Granja, F.; Moran-Lopez, J. L. Direct enumeration of the geometrical characteristics of clusters. *Nanostruct. Mater.* **1997**, *8*, 269−287.

DOI: 10.1021/acscatal.9b02079
ACS Catal. 2019, 9, 7124−7136